Estimating the Vertical Component of Water Velocity from Measurements Collected with a Free-fall Vehicle

DAVID C. JACOBS AND CHARLES S. COX

Scripps Institution of Oceanography, Ocean Research Division, La Jolla, California

(Manuscript received 11 October 1990, in final form 16 July 1991)

ABSTRACT

Estimates of the vertical component of water velocity are made with measurements of the pressure-change rate and rotation rate recorded by the free-fall vehicle "Cartesian diver" (CD). Using buoyancy control, this device moves alternately up and down, essentially at its terminal velocity through the surrounding water. Four angled wings fix the lift and rotational characteristics of the instrument. The rate of rotation is directly proportional to the terminal velocity of the instrument and is not sensitive to vertical water accelerations except at scale lengths somewhat less than the instrument height. When the pressure distribution is hydrostatic, the pressure-change rate is proportional to the sum of the instrument's terminal velocity and the vertical water velocity. Because the terminal velocity is a function of the instrument buoyancy, which varies slowly with depth, the fluctuations in vertical water velocity are well resolved by the fluctuations of the pressure-change–rate sensor. The orbital velocity of barotropic surface waves does not contribute to these measurements because isobars remain very nearly fixed to water particles. The vertical velocity of baroclinic flows, whether associated with internal waves, turbulence, or convective motions, is detectable in principle. Data from repetitive profiles over the depth range from 100 to 350 m are used to estimate the vertical components of velocities with a resolution of 0.1 mm s^{-1}. It is shown that at high frequencies, in a band centered near 0.1 Hz, a pressure disturbance caused by the nonlinear interaction of opposed surface wave trains is sometimes prominent and essentially limits the detection of short vertical wavelength internal motions to 2 m (the maximum vertical distance traveled in 10 s). In open-sea observations in both the Atlantic and Pacific, root-mean-square (rms) vertical velocities of 3–4 cm s^{-1} at vertical scales of 20 m and greater are commonly observed along with fluctuations of 1–10 mm s^{-1} with vertical scales down to 2 m.

1. Introduction

There are various methods to measure vertical velocity with differing resolutions, scale lengths, and measurable frequencies. One technique uses the time-depth variations of temperature isotherms to indirectly measure vertical velocity (Pinkel 1981). Some direct point measurements have been obtained through the use of neutrally buoyant floats with tilted vanes (Voorhis 1968) and moored triaxial propellers (Eriksen 1978). More recently, Doppler sonars have been used to give near-instantaneous velocity measurements along the axes of their beams (Plueddemann 1987; Sherman 1989). Moum (1990) has developed a microscale vertical velocity sensor using a Pitot tube mounted on a falling profiler to measure scales between 0.02 and 2 m.

The work we have done follows that of Desaubies and Gregg (1978), who first described the use of pressure-difference measurements from free-falling vehicles as a means to measure vertical velocity. They found that some of the fluctuations in the fall rate, as measured by a pressure gauge, represented the vertical velocity of the water rather than variations in the instrument's motion.

We have developed sensors for the free-fall vehicle Cartesian diver (CD) to measure the pressure-change rate and the rotation rate (an indication of the terminal velocity) with much greater resolution than previously obtained. We also consider the scales of errors from pressure fluctuations not associated with vertical water motions.

The vertical velocity of the instrument in a fixed frame of reference, w_{abs}, can be thought of as the sum of two velocities: the vertical velocity of the surrounding water and the terminal velocity of the instrument within the surrounding water. Figure 1 is a drawing showing the instrument moving with a terminal velocity w_{tv} within a reference frame that is moving with the vertical water velocity w_i, relative to a fixed surface. The measurement of vertical water velocity relies on our ability to accurately measure the absolute velocity of the instrument relative to a geopotential surface minus the terminal velocity of the instrument ($w_i = w_{abs} - w_{tv}$). This method is an accurate measurement of vertical water velocity as long as: 1) the terminal velocity is mainly a function of the buoyancy and drag

Corresponding author address: Dr. David C. Jacobs, Scripps Institution of Oceanography, Ocean Research Division, A-030, La Jolla, CA 92093.

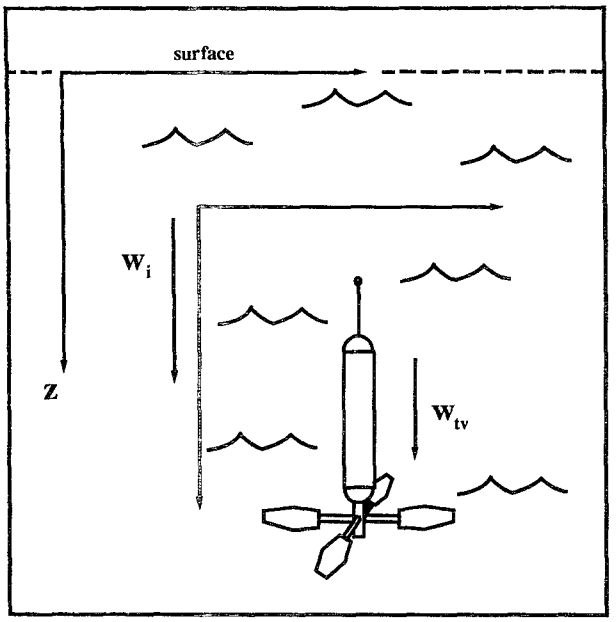

FIG. 1. A schematic depiction of the Cartesian diver's vertical velocity through the water column. The instrument has a velocity relative to the sea surface that is the sum of the velocity of the parcel of water immediately surrounding the instrument, w_i, and the terminal velocity of the instrument, w_{tv}, which is set by the net buoyancy of the instrument.

forces and not affected by vertical water accelerations $\partial w_i/\partial t$, and 2) the pressure field is hydrostatic.

A description of the instrumentation is given in section 2. Section 3 describes the measurement of the instrument's absolute vertical velocity w_{abs} and the terminal velocity w_{tv} including a discussion of the limitations and errors associated with each. Sections 4 and 5 conclude the paper with observations and a discussion.

2. Instrument description

The Cartesian diver profiling device has a cylindrical pressure case of radius 11.4 cm with a length (including endcaps and drop weight) of approximately 3 m. The cylinder axis remains vertical within a fraction of a degree during its motion. Four propeller-like vanes angled at 45° to the vertical have a wingspan of 1.6 m (Fig. 2) and force the instrument to rotate as it falls and rises between typical depth intervals of 50–350 m. It is autonomous and uses discrete buoyancy changes to reverse its direction of motion at chosen depth intervals. Data are recorded internally on a disk drive. In addition to active buoyancy control (using a piston and motor assembly), a passive pressurized volume of dry nitrogen is allowed to compress with depth in order to make the total compressibility of the instrument similar to seawater. This reduces the effect that the changing buoyancy of the instrument relative to seawater would have on the terminal velocity. A description of the mechanics of the instrument is contained in Duda et al. (1988), although many of the components have been upgraded and several new sensors have been installed. A discussion of the updates is in Jacobs (1989).

Four sensors are used to calculate the vertical water velocity versus depth: a pressure-change–rate sensor, a compass, an angular accelerometer, and an absolute pressure gauge. The pressure-change–rate sensor measures the vertical velocity of the instrument relative to the surface. The compass and angular accelerometer are used to infer the terminal velocity of the instrument relative to the water volume immediately surrounding it. The absolute-pressure gauge gives depth information as well as a second independent coarse measurement of the instrument's vertical velocity relative to the surface.

a. Pressure-change–rate sensor

A differential pressure sensor was used for the low-frequency (less than 0.1 Hz) measurement of the absolute velocity of the instrument relative to the sea surface. The transducer is a temperature compensated silicon diaphragm-type sensor (33 000 Pa full scale), which is mounted between two fluid-filled chambers, as shown in Fig. 3. Both chambers are filled with a nonconducting 0.3 Pa s viscous silicone oil. One chamber has an input through a flexible covering to seawater pressure. The second is a sealed reference chamber with a controlled leak into the first chamber via a 2-cm-long hypodermic needle. With a typical instrument fall rate of 15 cm s^{-1} and a time constant of nearly 4 s, there are not any pressure differences exceeding 60 cm of water (or equivalently, 6000 Pa). This is well within the full-scale rating of 33 000 Pa for the sensor. To protect against excessive pressures likely during deployment or recovery, two opposing pressure relief valves rated at 33 000 Pa were installed between the reference chambers. Depending on the sign of the pressure difference, one or the other valve opens to prevent sensor damage during large pressure differences.

The hypodermic needle–reference chamber system behaves as a differentiator for low-frequency pressure signals. The time constant is determined by the physical characteristics of the needle, oil, and chamber. Cox et al. (1984) detail the derivation for the equations and time constant for any given system. For external pressure variations of the form $P_o(\omega)\exp(i\omega t)$, the amplitude of the pressure difference recorded is

$$S(\omega) = P_o(\omega)\frac{i\omega\tau}{1 + i\omega\tau},$$

$$\tau = \frac{8k_f V_c \eta L}{\pi r^4}, \qquad (1)$$

where V_c = chamber volume, r = inner radius of needle,

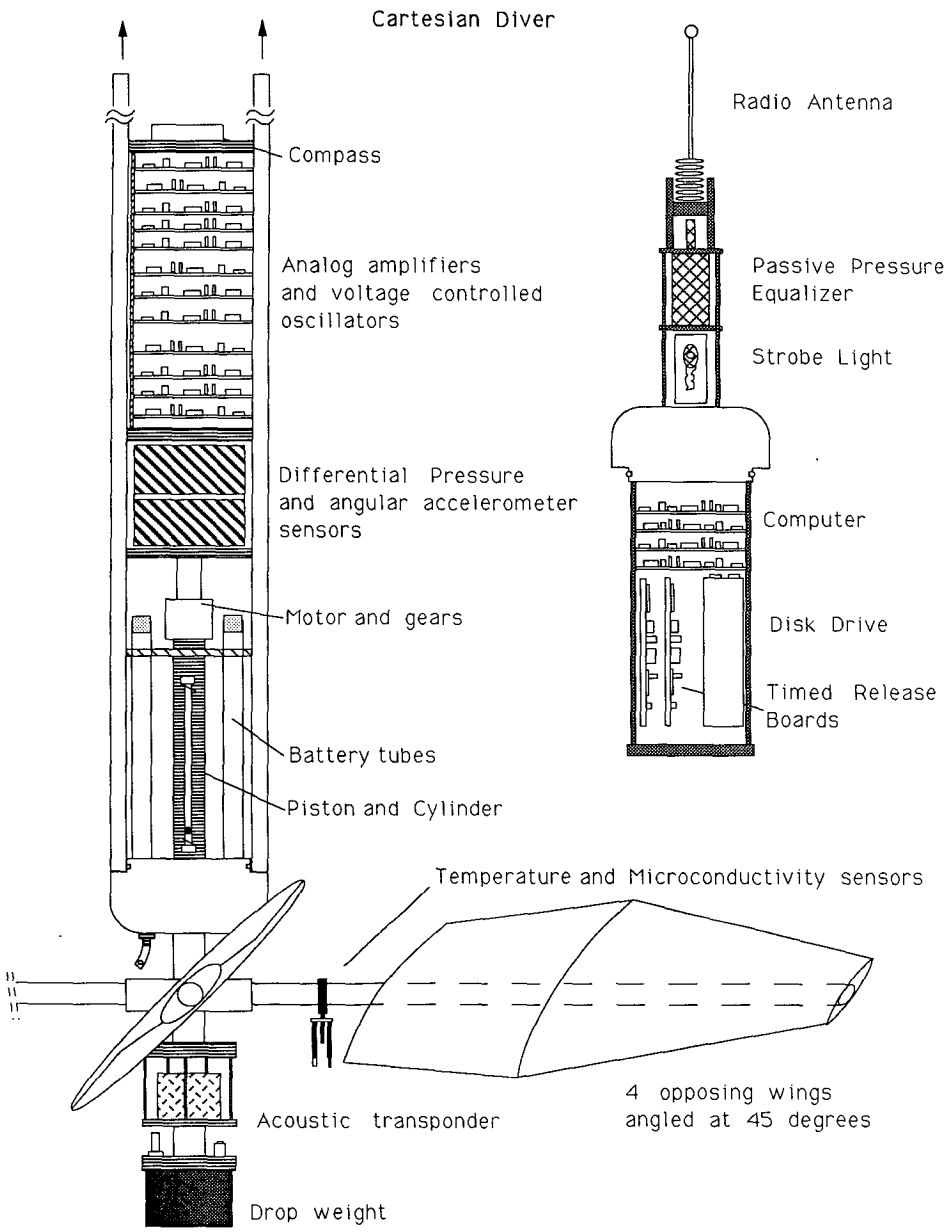

FIG. 2. Diagram of the major components of the Cartesian diver divided into its top and bottom sections.

L = needle length, η = fluid viscosity, and k_f = adiabatic compressibility of the silicone oil. Laboratory measurements of the decay time responses of the sensor to step functions in pressure give a measured value of τ equal to 3.72 s with a standard deviation of 0.19. At low frequencies such that $\omega\tau \ll 1$,

$$S(\omega) = i\omega\tau P_o(\omega). \quad (2)$$

This implies at low frequencies that the differential pressure signal is proportional to $\tau(\partial P/\partial t)$, which, if the pressure is hydrostatic, is equivalent to $\rho_o g\tau$ times the absolute fall speed of the instrument relative to the surface. The approximation (2) underestimates the pressure-change rate with increasing frequency as the measurement becomes more nearly a function of pressure rather than of the pressure-change rate. The amplitude weighting error in the transfer function between the pressure measured across the sensor and the rate of change of seawater pressure is shown in Fig. 4. In principle, this high-frequency error can be corrected, but currently, only frequencies below 0.1 Hz have been examined.

The average of the known changes in velocity between the ends of falling profiles and the beginnings

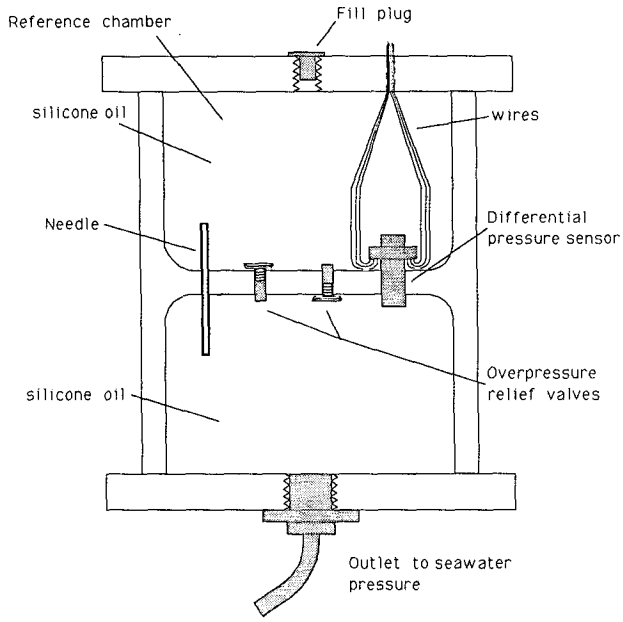

FIG. 3. Diagram of the two-chamber pressure case and sensor used to deduce the pressure-change rate of the falling instrument. The lower chamber has a direct input from the pressure in the ocean. The upper chamber is a reference chamber with a controlled leak through a hypodermic needle to the lower chamber.

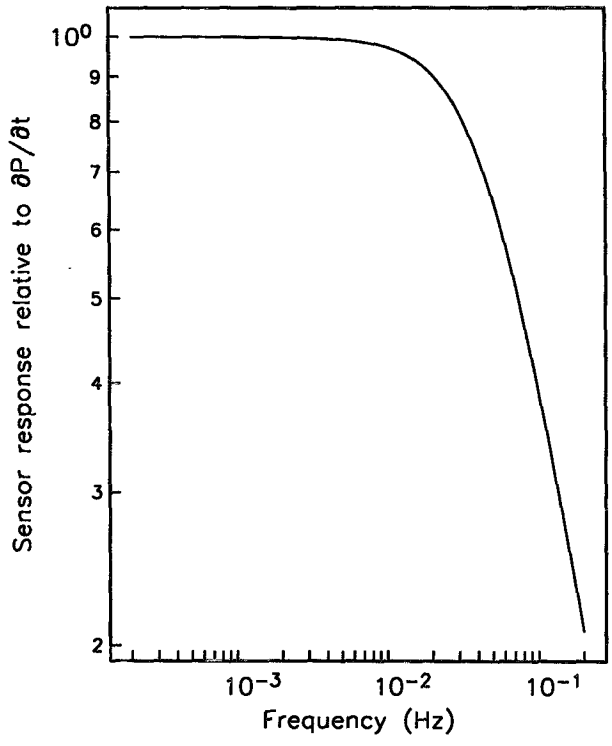

FIG. 4. The amplitude response is shown relating the pressure signal from the transducer with the rate of change of pressure outside the instrument. At low frequencies, the transducer pressure signal is directly proportional to the rate of change of pressure outside the instrument case.

of rising profiles are used to calibrate the pressure-change-rate sensor in units of meters per second (or equivalently pascals per second). These were the times during the deployment with the greatest instrument velocity change over the shortest time intervals. The short time interval minimizes errors induced by temperature or by changing vertical water velocities. The calibrated least count of the electronics corresponds to a vertical velocity resolution of 0.007 mm s^{-1} or 0.07 Pa s^{-1}. Figure 5 shows a comparison of a spectrum of vertical velocity from a typical profile with that of a spectrum collected with the instrument on a stationary bench at room temperature.

Temperature effects on the pressure-change-rate sensor. The sealed reference chamber makes the pressure-change-rate device susceptible to pressure errors from the significant thermal expansion coefficients of the silicone oil and aluminum housing. Cox et al. (1984) show that for slow changes of temperature, the error pressures induced in the enclosed volume of the reference chamber (not including the frequency-dependent factor due to the leak through the needle, which would reduce the effect at low frequencies) would be

$$P_f = \frac{\alpha_f T_f - \alpha_c T_c}{K_f + K_c}, \tag{3}$$

with α_f and α_c being the thermal volume expansion

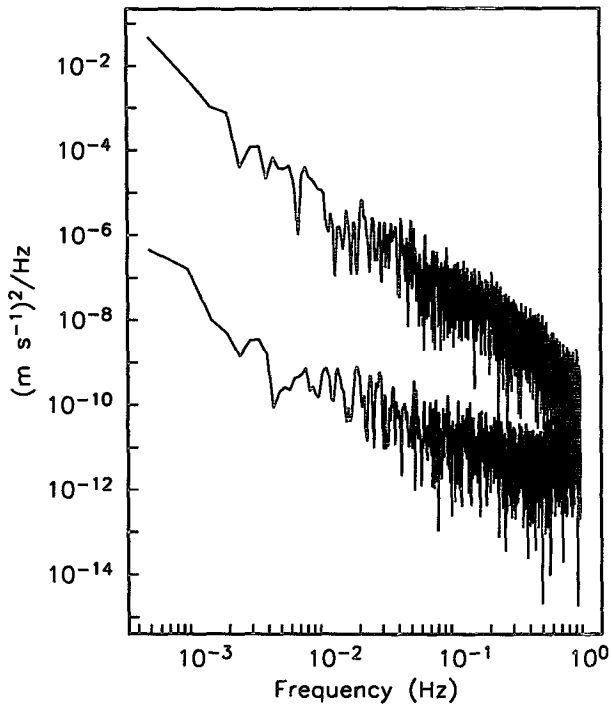

FIG. 5. A spectrum of vertical water velocity (upper curve) collected during a recent deployment is shown with a noise spectrum (lower curve) collected with the instrument on a fixed surface in a laboratory with limited temperature fluctuations.

coefficients of the silicone oil and aluminum case respectively, T_f and T_c the temperature, and K_f and K_c the compressibility. This is an idealized expression assuming that the temperatures are uniform in the case and fluid, respectively. The dominant ratio α_f/K_f is the order of 10^6 Pa °C^{-1}. Thus, it is expected that temperature variations could induce large spurious pressure fluctuations. Polyurethane foam, the air inside the pressure case, and the pressure case itself act together as a low-pass temperature filter by insulating the reference chamber from outside temperature fluctuations. Figure 6 shows the pressure-change-rate spectrum (during a calibration test) expressed in terms of velocity several minutes after a 13°C temperature drop at the outer skin of the instrument. A comparison of the spectrum in Fig. 6 with the room temperature bench spectrum in Fig. 5 shows that temperature-induced pressure fluctuations cannot be distinguished from the noise level above 2.0×10^{-3} Hz. Further, spectra measured before and up to 32 h after the temperature step show a similar response above 2.0×10^{-3} Hz. At lower frequencies, however, Fig. 6 shows the noise rising sharply. A temperature record (Fig. 7) collected over several complete cycles of the CD through its depth range shows large temperature fluctuations at frequencies comparable to the CD cycling frequency (approximately 2.0×10^{-4} Hz). To remove this error (which appears as a low-frequency drift), we compute a filter to convolve with the temperature data by measuring the velocity-sensor response to a controlled temperature step.

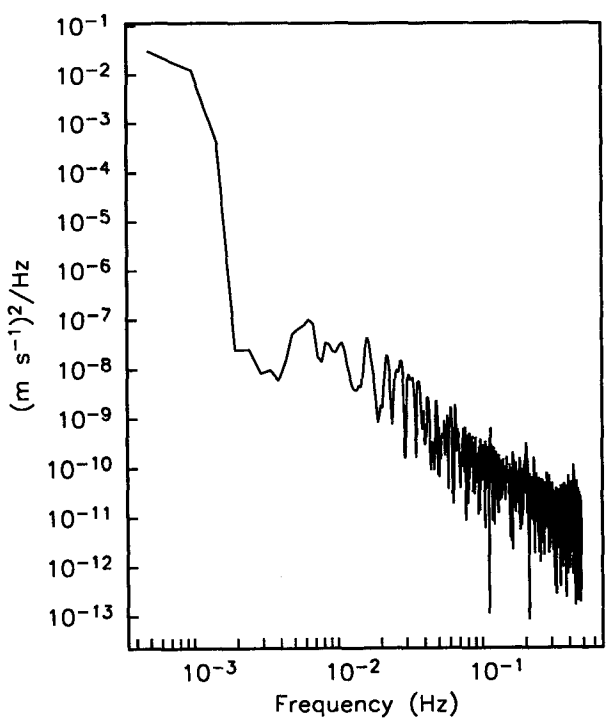

FIG. 6. A laboratory noise spectrum from the vertical velocity sensor is shown during a calibration test where the instrument was submerged in a chilled water bath. Low-frequency noise levels increase significantly above those in Fig. 5 due to the expansion and contraction of the reference chamber oil from the slowly diffusing temperature fluctuations. Because the noise is correlated with the outside temperature fluctuations, it can be removed.

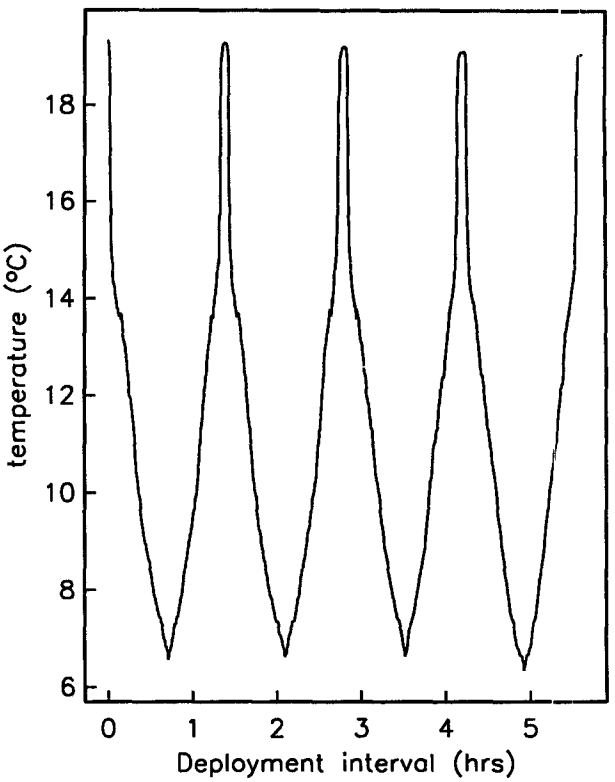

FIG. 7. Temperature data during a deployment is shown covering four complete cycles of the instrument through the depth range between 30 and 380 m.

By submerging the CD in a chilled water tank, we were able to approximate a step function in external temperature. The temperature and vertical velocity-sensor time series are shown in Fig. 8. We generate a numerical filter by inverse transforming the ratio of the Fourier transform of the first differenced time series. The shape of the filter weights is very close to the time series of the first-differenced velocity-sensor error response. After a deployment, the filter weights are convolved with the first-differenced temperature data, and the resulting series is integrated to obtain the correction terms. Figure 9 shows the effectiveness of the temperature correction scheme for both the chilled water example and a longer test using smaller room temperature fluctuations. The figure shows spectra of the vertical velocity-sensor noise (before and after removal of temperature effects) expressed in units of velocity from the two laboratory tests. The resulting noise levels are comparable and, integrated across the full bandwidth, are less than 0.1 mm s^{-1}.

This method leaves a residual error due to absolute temperature. Recently evidence has been found in the

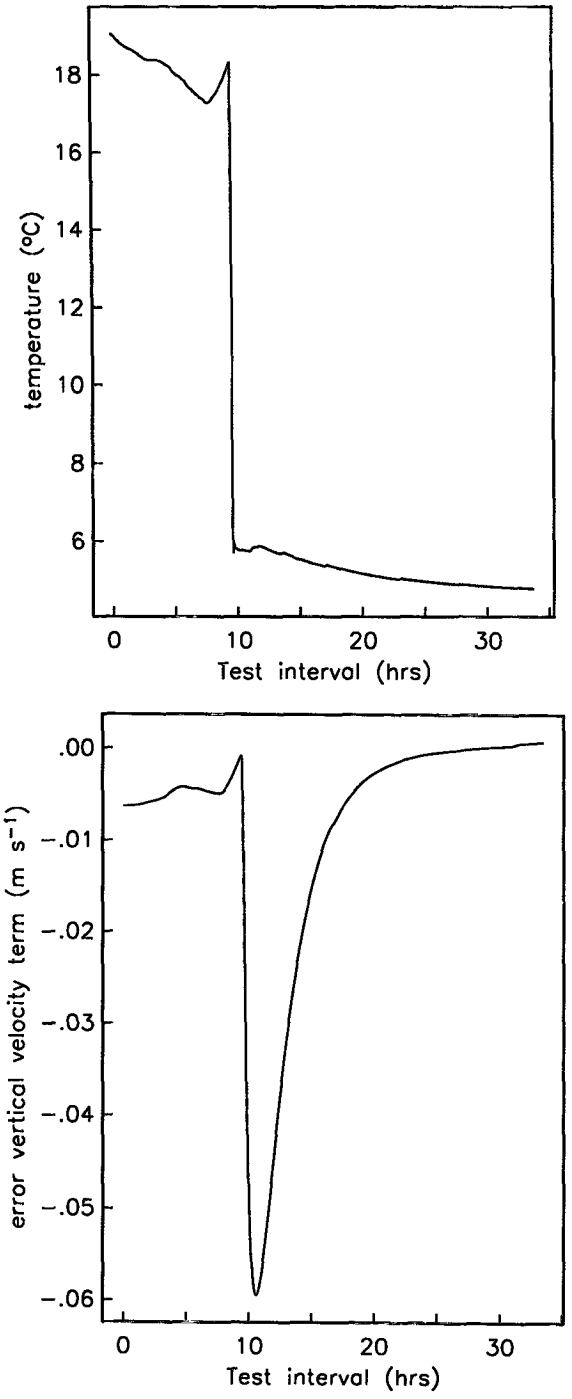

FIG. 8. (a) The temperature step recorded at the outside skin of the pressure case of the Cartesian diver during a calibration test where the instrument was submerged in a chilled water bath. (b) The resulting vertical velocity–sensor error.

laboratory that the differential-pressure–sensor outputs have a small absolute temperature dependence. This can be seen in the oceanic data by computing the difference between the low-passed vertical velocity series calculated from the absolute-pressure gauge and the temperature corrected low-passed velocity series calculated from the pressure-change–rate sensor. There remains an error versus depth that follows a closely repeated hysteresis loop for each complete dive cycle. The error is monotonic with depth and, for the last deployment where the temperature variation over the section was 13°C, the error magnitude slowly varied over a range of 2 cm s^{-1}. Installing a temperature sensor directly in the silicone oil of the reference chamber near the pressure sensor will provide the means to correct this problem, as well as to improve upon the corrections made with the outer temperature time series. Until then, we fit a fourth-order polynomial function to the hysteresis curve and subtract it from the vertical velocity–sensor data. The two low-passed vertical velocity measurements then agree within 0.5 mm s^{-1}.

b. Compass

A 10-bit, viscous damped Digi-Course magnetic compass with a least count of 6.136×10^{-3} rad was used to infer the low-passed rotation rate of the instrument. The CD rotates at an approximate rate σ_r of 0.26 rad s^{-1} with the angular position sampled at 0.25-s intervals. The data are first-differenced and a 32-s running-mean filter is used to give a low-passed resolution of $\pm 8.73 \times 10^{-5}$ rad s^{-1} for the local rotation rate assuming the preaveraged measurements were independent. There are error offsets for the angular position that do not affect the difference measurement but will be mentioned for completeness. The rotation speed introduces a lag in the measurement that is dependent on the viscosity of the oil in the compass. Further, the viscosity itself is dependent on the surrounding temperature. A linear relation between viscosity and temperature is assumed as a first-order correction. The lag in degrees for eight different rotation rates is measured at both 21.9° and 2°C and is found to follow the relation

$$y = (-27.27t + 1202.14)r, \qquad (4)$$

where y is the lag (deg), t is the temperature in degrees Celsius, and r is the rotation rate in hertz. Using this relation, the lag error is corrected for both rotation and temperature.

In addition, the CD usually has a small magnetic moment. We are trying to minimize it by placing the electronics and the battery supplies as far away from the compass as possible. It shows up in the first-differenced compass measurements as a constant magnitude sine wave that is phase locked to the radial position. It is easily removed from the data.

c. Angular accelerometer

The angular accelerometer is designed to correct the rotational measurements at time scales shorter than

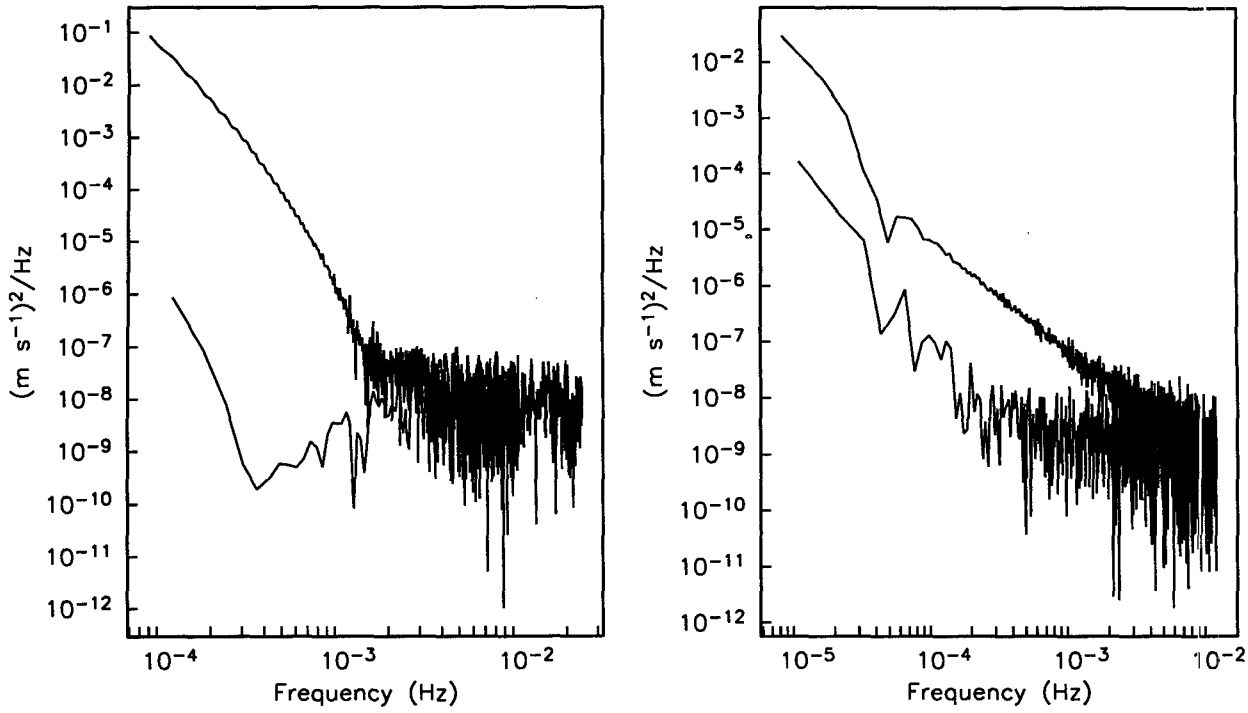

FIG. 9. (a) The upper curve shows the vertical velocity-sensor spectra from the chilled water bath test where the instrument was exposed to a large temperature step. The lower curve is the vertical velocity spectra for the same time interval after the temperature effects were removed with the correction filter. (b) Similar spectra as (a) but during a bench test lasting 2 days where the instrument was exposed to fluctuating room temperatures ranging approximately 3°C. The resulting noise levels are roughly equivalent to those in (a).

the filter length used on the first-differenced compass data when the error from the least count of the compass would obscure any high-frequency rotational changes. However, the data from the angular accelerometer shows only rare instances where the low-passed first-differenced compass measurements were not extremely accurate. The first deployment of the CD had only one such occurrence over the entire 60 profiles when something apparently became attached to the instrument. There was a large deceleration to nearly half the original rotation rate as the Cartesian diver adjusted to its new buoyancy and drag. Twenty meters later, a large acceleration restored the instrument to its original rotation rate.

A schematic diagram of the angular accelerometer is shown in Fig. 10. The output is from a differential-pressure sensor with a 6600-Pa full-scale output. The gauge is connected to one end of a thin, rigid, fluid-filled tube 62.2 m in length with an inner diameter of 0.62 mm, which is wound around a short section of plastic pipe of radius 8.25 cm giving 120 windings. The opposite end of the tube is then folded back and connected to the opposite end of the pressure sensor, making it a closed system. The plastic pipe's axis is mounted along the vertical axis of the diver so that any rotational acceleration generates a differential pressure across the sensor. Carbon tetrachloride is chosen for the fluid because of its low viscosity (about 10^{-3} Pa s) and high density (1.6×10^3 kg m^{-3} at 0°C). The relation between the differential pressure seen across the gauge and the angular acceleration (neglecting viscous effects) is

$$\Delta P = \rho l R \theta_{tt}, \tag{5}$$

where R = radius of loop, l = length of pipe, θ_{tt} = angular acceleration (rad s^{-2}), ρ = density of fluid, and ΔP = differential pressure. With $l = 2\pi r N$ (N is the number of windings), then

$$\Delta P = \theta_{tt}(8.1847 \times 10^{-3} \text{ Pa s}^2). \tag{6}$$

In practice, a pressure resolution of 0.2 Pa corresponding to an angular acceleration resolution of 2.4×10^{-5} rad s^{-2} is achieved.

The derivation of (5) neglects the importance of viscosity and is a good approximation as long as the pressure term due to the viscous force is negligible compared to the acceleration term. Viscosity is a consideration because the fluid filling the accelerometer tube flows in response to angular accelerations. There are three mechanisms that will cause flow: compliance of the pressure sensor, elasticity of the walls of the tube, and compressibility of the fluid. The sensor compliance is considered negligible. The expansion of the tube subjected to a pressure difference from the inner to outer diameter can be calculated using the relations for plane deformation (Sokolnikoff 1956). The effect

of this expansion and of the compressibility of the fluid can be evaluated as follows.

Let s be the distance measured along the tube ($s = 0, l$ are the two ends of the tube where flow vanishes owing to the negligible compliance of the differential pressure sensor), $r = 0.31$ mm is the radius of the tube, and $\eta = 10^{-3}$ Pa s is the viscosity. The equation relating pressure within the fluid $p(s, t)$, linear acceleration of the tube $a(t)$ equivalent to $R\theta_{tt}$, and averaged fluid velocity $u(s, t)$ relative to the tube is

$$\frac{\partial p}{\partial s} = -\rho a - \frac{8\eta u}{r^2}, \tag{7}$$

where the last term represents the contributions to the pressure gradient by Poiseuille's formula describing viscous flow through a pipe.

The linearized one-dimensional equation of continuity and the equation of state relating small density changes to small pressure changes can be combined to give

$$\frac{\partial p}{\partial t} = -\frac{1}{\Phi}\frac{\partial u}{\partial s}, \tag{8}$$

where $\Phi = 10^{-9}$ Pa^{-1} is a combined effect from the compressibility of the fluid and the expansibility of the tube.

We assume a time dependence, $\exp(i\omega t)$, and combining (7) and (8); the general solution is

$$u = A\exp(\beta s) + B\exp(-\beta s) - \frac{r^2\rho a}{8\eta}$$

$$\beta^2 = \frac{i\omega 8\eta\Phi}{r^2}. \tag{9}$$

The boundary condition $u = 0$ at $s = 0, l$ requires that

$$A = B \approx \frac{r^2\rho a}{16\eta}, \tag{10}$$

provided that $|\beta l| \ll 1$. Accordingly, the pressure gradient becomes

$$\frac{\partial p}{\partial s} = \frac{i}{\Phi\omega}\frac{\partial^2 u}{\partial s^2} \approx -\rho a[1 + 1/2(\beta s)^2]. \tag{11}$$

Hence the maximum relative error in (7) is $1/2|\beta l|^2$, which for the parameters of our device is 0.02 at the Nyquist frequency of 2 Hz. The errors become smaller at lower frequencies.

The initial calibrations were done on a rotating platter using step changes in velocity to generate approximate delta functions in acceleration. However, the final calibration used times during deployment when the diver became fouled temporarily and experienced sudden decelerations and accelerations whose time interval and size were well determined by the compass. This eliminated the need to use a convolving filter on the data but added an assumption that the response is linear over the frequencies of interest.

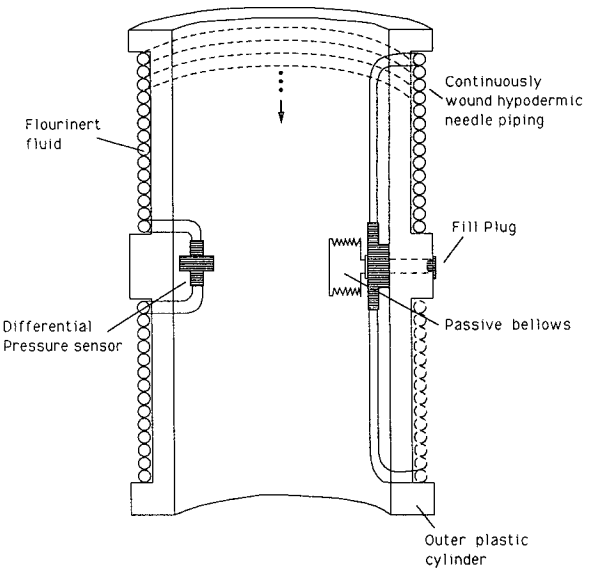

FIG. 10. Diagram of the angular accelerometer. A thin metal tube 62.2 m long is wound around a cylindrical pipe of radius 8.25 cm with the ends mated together with a differential pressure sensor. A passive bellows at the midpoint of the tube allows for thermal expansion of the fluid.

In actual use, the angular accelerometer is only used as a check against high-frequency accelerations (less than a minute), which the diver only rarely exhibits. The angular acceleration is very small at these frequencies during deployments with a typical total variance of 6×10^{-8} rad^2 s^{-4}.

d. Absolute-pressure sensor

The absolute-pressure gauge is used to record depth information and to give calibration checks for both the pressure-change–rate sensor and the compass. It is a temperature-compensated (0°–100°C) strain gauge Model P-703 manufactured by Shaevitz with a 6.6-MPa dynamic range. The signal is digitized to give a least count every 1 cm, although its maximum rated static error is 3 m. Calibration with a dead-weight tester at 15 pressure increments of 0.3295 MPa gives a linear correlation coefficient of $R = 0.99998$. Multiple measurements at each pressure level show a repeatability of the equivalent of ±5 cm of water.

3. Measuring vertical velocity

a. Absolute vertical velocity

The differential-pressure gauge is used to infer the absolute vertical velocity of the CD in the ocean. As the instrument moves through the water, the pressure-change rate as seen by the instrument is a complicated function of the time variations of the many pressure generating terms and their spatial variations that enter because the instrument is in motion. However, for our

situation, the dominant terms are hydrostatic. Thus, the pressure-change rate is that due to the sum of the instrument's local terminal vertical velocity w_{tv} with respect to the surrounding water and the vertical component of the velocity of the surrounding water, w_i (which is assumed to carry the diver with it). This can be expressed as

$$\frac{DP}{Dt} = -\rho_o g w_{abs} = -\rho_o g(w_{tv} + w_o). \quad (12)$$

To arrive at (12), we begin with the expansion of the substantial derivative. In addition to w_i, which is assumed to originate from internal waves, there is also a velocity w_s from surface waves. Thus, the expression is

$$\frac{DP}{Dt} = \frac{\partial P}{\partial t} + (w_{tv} + w_i + w_s)\frac{\partial P}{\partial z} + u\frac{\partial P}{\partial x}, \quad (13)$$

where $\partial P/\partial x$ is the pressure gradient along the direction of u (a representative maximum horizontal velocity of the diver). The pressure is

$$P = P_s + P_i + P_r - \rho_o g z \quad (14)$$

with the subscripts referring to: s—linear effects of surface gravity waves; i—internal waves; r—ram pressure. The hydrostatic pressure is $-\rho_o g z$. In addition, there are pressures from nonlinear interactions of surface waves that extend to great depths when there are opposed wave trains at the sea surface (Longuet-Higgins 1950). Pressure disturbances of this type generate microseisms in the seabed and can propagate along the seafloor from distant sources. These nonlinear pressures will be eliminated by keeping the measurement below 0.1 Hz. Cox and Jacobs (1989) have made measurements of these pressures in midwater and show they can be quite large at frequencies above 0.1 Hz. Figure 11 shows a typical vertical velocity spectrum including the noise from the microseism peak.

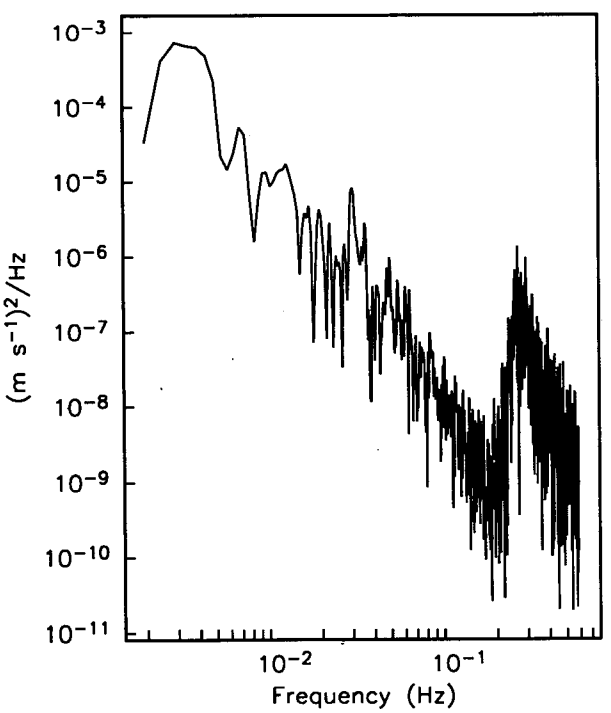

FIG. 11. A vertical water velocity spectrum taken in the open ocean during an interval where the microseism pressure fluctuations from the sea surface contribute errors that dominate the velocity spectrum above 0.1 Hz.

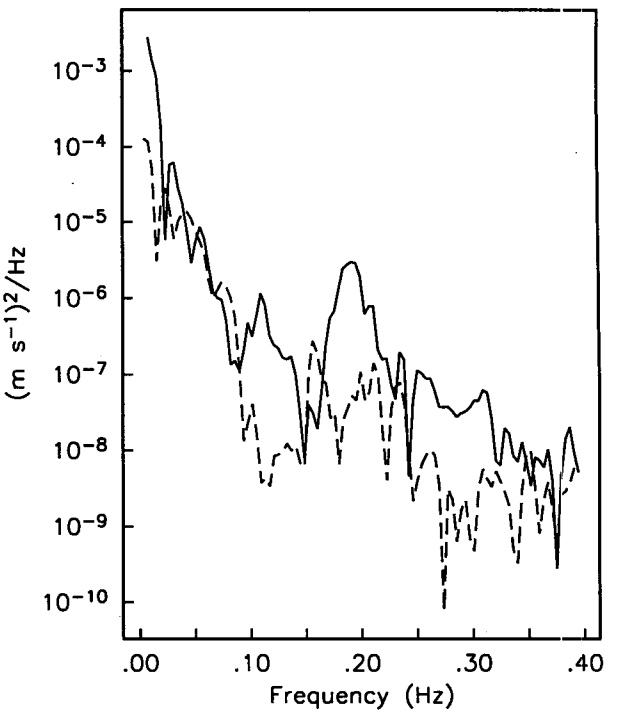

FIG. 12. Shown are spectra of vertical water velocity for two depth intervals. The solid curve represents data collected during one section between 40 and 70 m. The dashed curve represents data collected from the same section between 100 and 140 m. The band between 0.08 and 0.15 Hz for the solid curve would be four orders of magnitude bigger as estimated from shipboard visual observations of the wave height if the diver's vertical velocity sensor included error fluctuations from linear surface wave pressures.

To examine the relative size of the terms in (13), the maximum value for the ram pressure along a body and the linear sinusoidal wave trains for the wave pressures and velocities are used. The result is

$$P_s = -\rho_o g \eta_o \cos(k_s x - \sigma_s t)\frac{\cosh[k_s(z+h)]}{\cosh(k_s h)}$$

$$w_s = \sigma_s \eta_o \sin(k_s x - \sigma_s t)\frac{\sinh[k_s(z+h)]}{\sinh(k_s h)}$$

$$P_i = -\rho_o q_i \sigma_i \frac{m_i}{k_i^2}\exp[i(k_i x + m_i z - \sigma_i t)]$$

$$w_i = q_i \exp[i(k_i x + m_i z - \sigma_i t)]$$

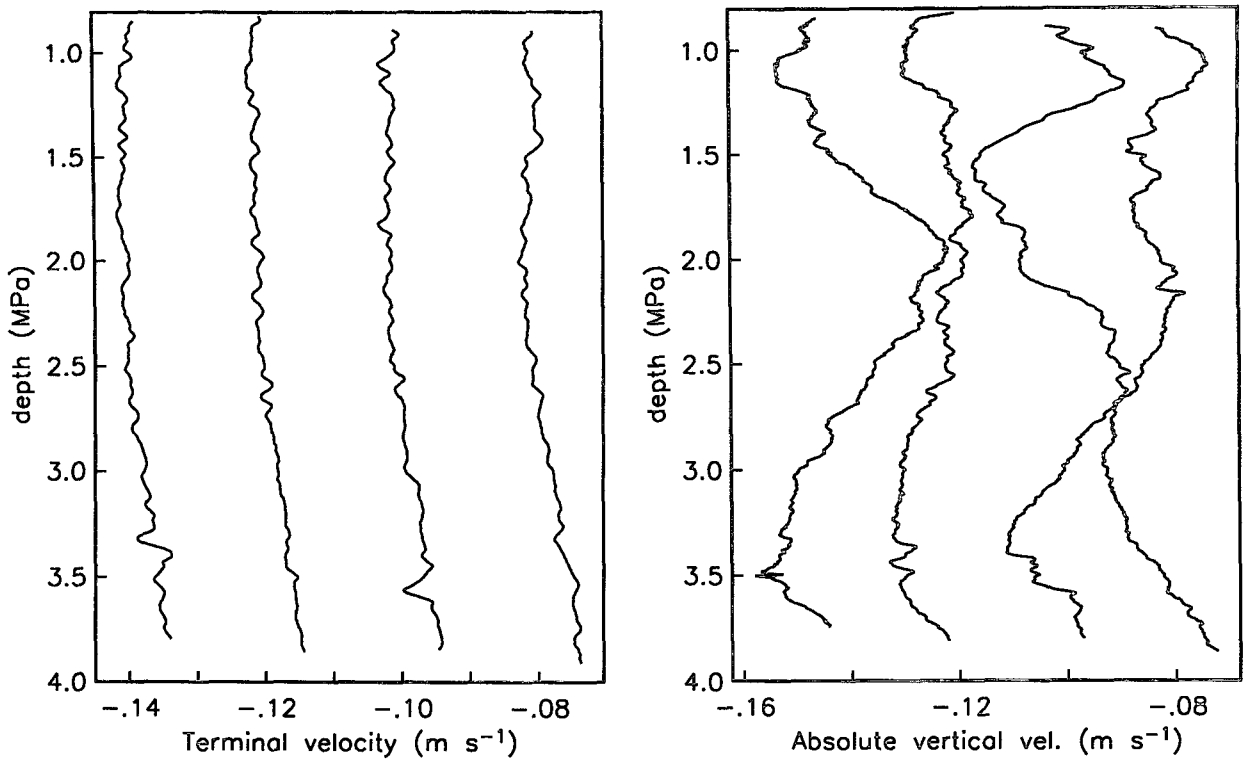

FIG. 13. (a) Compass-derived measurements of the terminal velocity of the instrument relative to the surrounding water are shown for four successive falling sections. They are offset from each other for clarity. (b) Similarly offset measurements of the absolute velocity of the instrument for the same four sections. The difference of the two measurements is the vertical water velocity.

$$P_r = \frac{1}{2}\rho_o w_{tv}^2$$

$$\frac{\partial P_r}{\partial t} = \rho_o w_{tv}\frac{\partial w_{tv}}{\partial t}, \tag{15}$$

where η_o, k_s, and σ_s are surface wave amplitude, horizontal wavenumber, and radian frequency, respectively; h is absolute value of water depth; and z is measured positive upward with $z = 0$ the surface. Also, q_i, k_i, m_i, and σ_i are internal vertical wave velocity amplitude, horizontal and vertical wavenumber, and radian frequency, respectively.

If a minimum desired resolution of 0.1 nm s^{-1} is assumed for $w_{tv} + w_i$ in (12), it must be shown that the additional terms in (13) do not contribute signals of that magnitude. Our biggest concerns, especially at shallower depths, are the linear surface wave pressure-change rate $\partial P_s/\partial t$ and the surface wave orbital velocity term $\rho_o g w_s$. However, these first-order terms almost exactly cancel each other except very near the ocean bottom (where they are negligible anyway) as long as the diver follows the vertical orbital motions of the surface waves at any given depth. Figure 12 shows spectra of the diver's vertical velocity for two depth intervals: 30–70 m and 100–140 m. If all the difference in the band between 0.08 Hz and 0.15 Hz is assumed to be residual signals from the surface waves, the integrated error is less than 0.1 mm s^{-1}.

The other first-order terms are the time derivatives of the internal wave pressure and the ram pressure. The rate of change of the internal wave pressure is typically 10^{-4} the size of the hydrostatic term $\rho_o g w_i$, which means that the internal wave velocities would have to exceed 1000 mm s^{-1} before the errors would exceed 0.1 mm^{-1} at any given frequency. The rate of change of the ram pressure is mostly influenced by the rate of change of the diver's terminal velocity, which is very small. A typical error velocity of 10^{-3} mm s^{-1} is induced by the ram-pressure variations.

Of the second-order terms, the largest are $w_{tv}(\partial P_s/\partial z)$ and $u(\partial P_s/\partial x)$. At depths greater than 100 m, a swell frequency of 0.1 Hz, a wave amplitude of 10 cm, terminal vertical velocity for the diver of 15 cm s^{-1}, and a horizontal velocity of 50 cm s^{-1}, the maximum error in the vertical velocity measurement for both terms is less than 0.1 mm s^{-1}.

Thus, at frequencies below 0.1 Hz and depths greater than 100 m, the pressure signal across the sensor can be directly associated with the absolute fall speed of the instrument relative to a geopotential level surface with maximum signals from other nonhydrostatic pressure effects typically less than 0.1 mm s^{-1}.

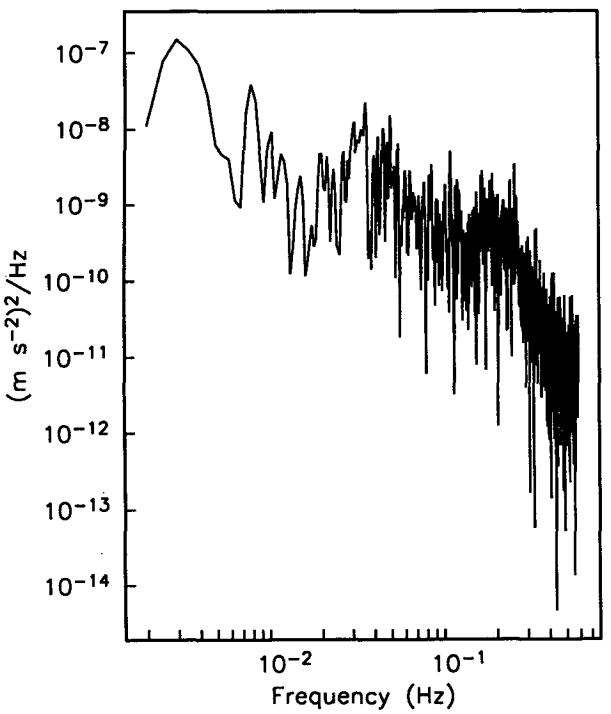

FIG. 14. Using the measured proportionality constant between rotation and vertical travel, a typical spectrum of the vertical accelerations of the instrument is shown using the angular accelerometer. The small accelerations illustrate the smooth nature of the rotation rate and, consequently, the terminal velocity at short time scales.

b. *Instrument terminal velocity in a local water volume*

The terminal velocity of the diver through the local surrounding water is inferred from measurements of the rotation rate of the instrument as it spins under the influence of four angled wings. Numerical and scaled laboratory studies done by Mortensen and Lange (1976) and oceanic measurements taken by Desaubies and Gregg (1978) using similar winged instruments have shown that the rotation rate σ_r is directly proportional to the terminal velocity w_{tv}. This remains true even given the complicated geometries of the wings and the instrument case. Further, they also show that the terminal velocity is a function of the buoyancy and drag forces and is not sensitive to vertical water accelerations. This insensitivity to the forces caused by vertical accelerations will of course break down at small enough vertical scales such that the forces vary significantly over the length of the instrument. However, since most of the vertical friction is concentrated at the wings, the actual minimum vertical scale may be much shorter.

Tilts caused by vertical shear were also considered by Simpson (1972), Mortensen and Lange (1976), Desaubies and Gregg (1978), and Duda et al. (1988). For even appreciable shears, a maximum bound of 0.1° tilt was either measured or calculated for each of the instruments. Duda et al. (1988) did a calculation of the tilt of the CD based on Evans et al. (1979), resulting in an upper bound of 0.03°. Using this upper bound, and assuming a terminal speed of 15 cm s^{-1} along the tilted path, the error in the true vertical terminal speed of the instrument is negligibly small. However, if the CD tilts and then slides along the plane parallel to the wings under the influence of a large horizontal velocity, the effect is much greater. Using the same upper bound on the tilt and a horizontal velocity of 50 cm s^{-1}, the error is as large as 0.2 mm s^{-1}. This type of error would only occur in regions of large vertical shear. As long as the tilt does not remain over the averaging length of the compass or velocity sensor data, the average resolution will still be better than 0.1 mm s^{-1}.

The proportionality constant between the CD rotation rate and the terminal velocity is measured by averaging the total rotations as measured by the compass for each rising and falling profile over the known depth change as measured by the absolute-pressure gauge. The standard deviation of the resulting average is equivalent to an absolute terminal velocity error of

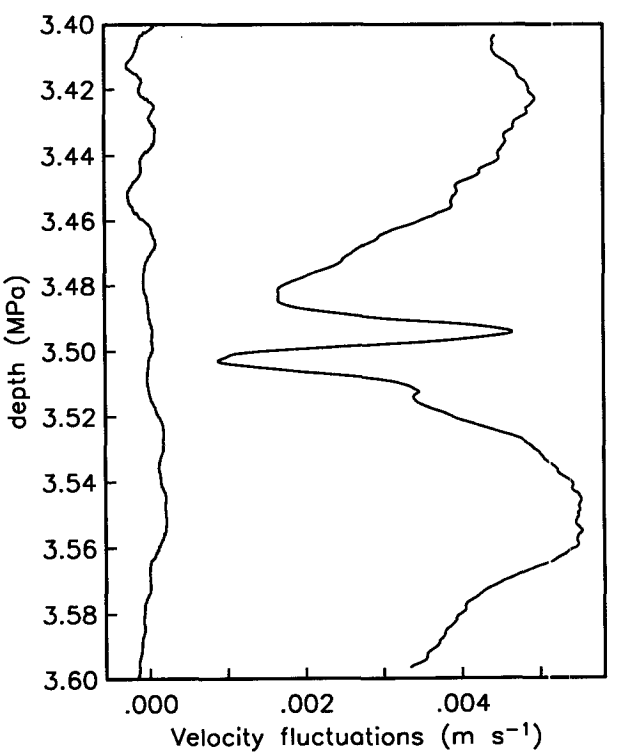

FIG. 15. The velocity fluctuations over a 20-m interval are shown. The leftmost curve is the integrated accelerometer data showing the small-scale fluctuations in the terminal velocity of the instrument. The right-hand curve shows the absolute vertical instrument velocity over the same interval. Even for scales smaller than 2 m, the terminal velocity remains insensitive to rather sharp fluctuations in the absolute velocity.

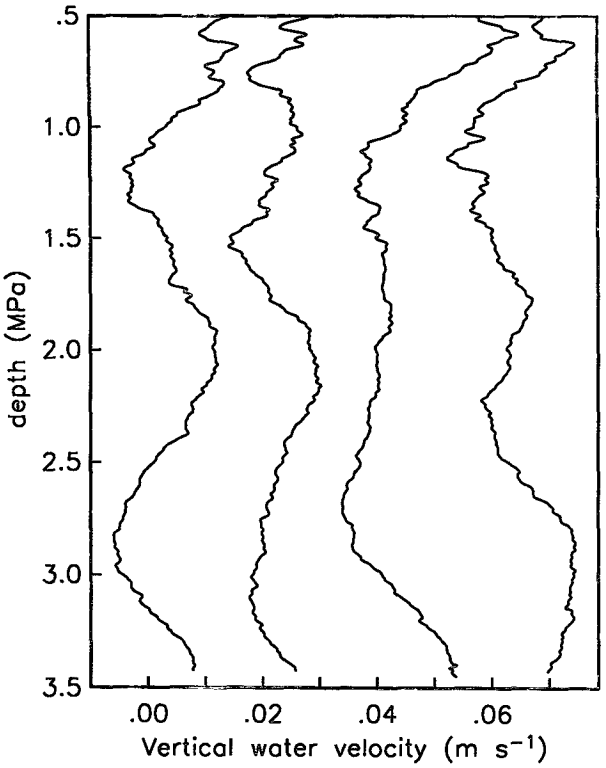

FIG. 16. Vertical sections of vertical water velocity as measured by the Cartesian diver. The profiles are offset horizontally for clarity and represent sequential downward excursions spaced approximately 80 min apart. The data was collected in the open ocean of the Pacific 400 km west of San Diego.

± 0.1 mm s^{-1}. Using the measured proportionality constant, the resolution as determined in section 2a becomes ± 0.05 mm s^{-1}. Evidence that the compass derived terminal velocity is only a function of the relative buoyancy between the CD and the seawater can be seen in Fig. 13. Successive sections of the terminal velocity show slow velocity changes with depth from section to section consistent with slow buoyancy changes. This contrasts with the same successive sections of the absolute vertical velocity, which show much greater variability.

The angular accelerometer is used to examine the smoothness of the rotation rate (and thus, terminal velocity) at time scales of less than 1 min. It has a vertical acceleration resolution of 1.4×10^{-5} m s^{-2}. The accelerations are relative to the local water volume surrounding the instrument. A typical spectrum of vertical accelerations (Fig. 14) measured in the Atlantic over a several-minute interval provides further evidence of the smoothness of the terminal velocity of the instrument. This does not imply that the instrument is not responding to changes in the vertical velocity of the water. While the terminal velocity remains relatively constant, the absolute velocity varies significantly over many scales (Fig. 13). This implies that the instrument and the surrounding water are being accelerated together. As mentioned earlier, if the vertical water accelerations are over scales much shorter than the instrument, the CD will not be able to accelerate with the water. By comparing variations in the absolute vertical velocity measurements with variations in the short time-scale terminal velocity as determined by integrating the angular accelerometer data, an attempt to estimate the actual minimum vertical scale where vertical accelerations begin affecting the terminal-velocity measurements can be made. Figure 15 shows that for changes in the vertical water velocity at scales significantly less than 2 m, there are only minimal changes in the terminal velocity measurements. A shorter scale length example was not found in the data.

4. Observations

Data have been collected in the Pacific about 400 km west of San Diego in 3.7-km-deep water. Figure 16 shows successive profiles of vertical velocity horizontally displaced. The repetition period between profiles is approximately 1.5 h. Figure 17 shows data collected in the Atlantic 250 km east of Chesapeake Bay in similar depth water. The dominant features are large

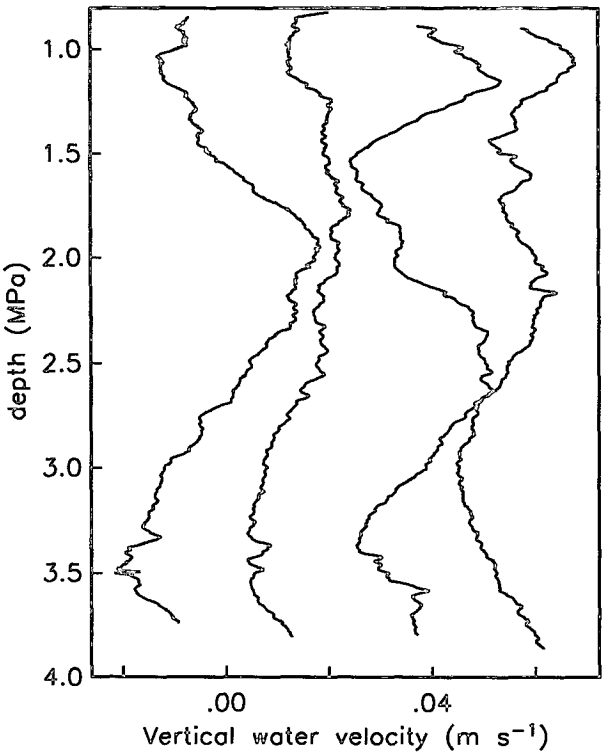

FIG. 17. Vertical sections of vertical water velocity similar to those in Fig. 16 collected in the North Atlantic 250 km east of Chesapeake Bay.

magnitude (20–40 mm s^{-1}) fluctuations of apparent 50–200-m wavelength. The disparity from profile to profile indicates high-frequency waves relative to the repetition rate of the profiles. There is a strong possibility that they have much longer vertical wavelengths than what is seen in the data that are being aliased by the slow fall speed of the CD. From other deep ocean measurements (Pinkel 1981) using high-speed CTD profiles, there is evidence that large magnitude near-Väisälä frequency waves of 1 km or greater wavelength are common. Figures 16 and 17 also shows many small-scale features of smaller magnitude distributed over many scales and magnitudes.

5. Discussion

A compass, an angular accelerometer, and a differential-pressure sensor, suitably insulated from temperature, are combined on a slow and smoothly falling profiler (the Cartesian diver) to measure the vertical component of the water velocity at a vertical resolution of approximately 2 m. The small-scale resolution is determined mostly by nonlinear pressure signals from surface waves (microseisms), which obscure signals at recording frequencies greater than 0.1 Hz (approximately less than 2 min vertical distance). Temperature errors at large scales can significantly affect the accuracy if not compensated. At depths greater than 100 m, the velocity resolution is better than 0.1 mm s^{-1}, with an apparent accuracy of better than 0.5 mm s^{-1} using the low-passed velocity measured with the absolute-pressure gauge as a reference.

Acknowledgments. This work was supported by the Office of Naval Research. Thanks are due to Tom Deaton, Jacques Lemire, and John Lyons for their help in the design and deployment of the Cartesian diver. Also, thanks to Agusta Flosadottir and to the reviewers for their helpful comments on the manuscript.

REFERENCES

Cox, C. S., and D. C. Jacobs, 1989: Cartesian Diver observations of double frequency pressure fluctuations in the upper levels of the ocean. *Geophys. Res. Lett.*, **16,** 807–810.

——, T. K. Deaton, and S. C. Webb, 1984: A deep-sea differential pressure gauge. *J. Atmos. Oceanic Technol.*, **1,** 237–246.

Desaubies, Y. J. F., and M. C. Gregg, 1978: Observations of internal wave vertical velocities by a free-fall vehicle. *Deep-Sea Res.*, **25,** 933–946.

Duda, T. F., C. S. Cox, and T. K. Deaton, 1988: The Cartesian Diver: A self-profiling Lagrangian velocity recorder. *J. Atmos. Oceanic Technol.*, **5,** 16–33.

Eriksen, C. C., 1978: Measurements and models of fine structure, internal gravity waves, and wave breaking in the deep ocean. *J. Geophys. Res.*, **83,** C6, 2989–3009.

Evans, D. L., H. T. Rossby, M. Mork, and T. Gytre, 1979: YVETTE—a free fall shear profiler. *Deep-Sea Res.*, **26,** 703–718.

Jacobs, D. C., 1989: Observations of vertical shear and Reynolds stresses in the main thermocline of the deep ocean and measurements of the near-field microseism pressure spectrum. Ph.D. thesis, University of California, San Diego, 105 pp.

Longuet-Higgins, M. S., 1950: A theory on the origin of microseisms. *Philos. Trans. Roy. Soc. London,* Ser. A, **243,** 1–35.

Mortensen, A. C., and R. E. Lange, 1976: Design considerations of wing stabilized free-fall vehicles. *Deep-Sea Res.*, **23,** 1231–1240.

Moum, J. N., 1990: Profiler measurements of vertical velocity fluctuations in the ocean. *J. Atmos. Oceanic Technol.*, 7(2), 323–333.

Pinkel, R., 1981: Observations of the near-surface internal wavefield. *J. Phys. Oceanogr.*, **11,** 1248–1257.

Plueddemann, A. J., 1987: Observations of the upper ocean using a multi-beam Doppler sonar. Ph.D. thesis, University of California, San Diego, 183 pp.

Sherman, J. T., 1989: Observations of fine-scale vertical shear and strain in the upper ocean. Ph.D. thesis, University of California, San Diego, 145 pp.

Simpson, J. H., 1972: A freefall probe for the measurement of velocity microstructure. *Deep-Sea Res.*, **19,** 331–336.

Sokolnikoff, I. S., 1956: *Mathematical Theory of Elasticity*. 2d ed., McGraw-Hill, 476 pp.

Voorhis, A., 1968: Measurements of vertical motion and the partition of energy in the New England slope water. *Deep-Sea Res.*, **15,** 599–608.